Recurrent large-scale solar proton events before the onset of the Wolf grand solar minimum

Hiroko Miyahara[1,2,*], Fuyuki Tokanai[3,4], Toru Moriya[4], Mirei Takeyama[4], Hirohisa Sakurai[3], Motonari Ohyama[5], Kazuho Horiuchi[6], and Hideyuki Hotta[7]

[1]Humanities and Sciences/Museum Careers, Musashino Art University, Tokyo 187-8505, Japan.

[2] Okinawa Institute of Science and Technology Graduate University, Okinawa 904-0495, Japan

[3]Faculty of Science, Yamagata University, Yamagata 990-8560, Japan.

[4]Center for Accelerator Mass Spectrometry, Yamagata University, Yamagata 999-3101, Japan.

[5]Botanical Gardens, Tohoku University, Miyagi 980-0862, Japan

[6]Graduate School of Science and Technology, Hirosaki University, Hirosaki, Aomori 036-8561, Japan.

[7]Department of Physics, Graduate School of Science, Chiba University, 1-33 Yayoi-cho, Inage-ku, Chiba 263-8522, Japan.

19   *Correspondence to miyahara@musabi.ac.jp

20

21   **Key points:**

22   ・Multiple abrupt increases in carbon-14 content were found during the transition

23   time of solar activity into the grand minimum state

24   ・They occurred at solar activity maximum or at the declining phase of solar

25   cycles, suggesting that they originate from solar proton events

26   ・The Wolf minimum may provide a unique opportunity to potentially deepen the

27   understanding of the solar dynamo

28

29

30   **Abstract**

31   Carbon-14 in tree rings have suggested that there had been multiple extreme

32   solar proton events (SPEs) in the past. While the largest events such as in 774–

33   775 CE can be significantly detected by the typical precision of accelerator mass

34   spectrometry, smaller but possibly more frequent events have been difficult to be

35   detected. Thus, the frequency or any characteristics of such relatively smaller

36   events are still largely unknown. In this paper, we report that multiple large SPEs

had occurred before the onset of the Wolf grand solar minimum based on high-precision carbon-14 analyses. It is suggested that they had occurred at the maximum and the declining phase of solar cycles, and that they had occurred during the transition time of solar activity into a deep minimum. We propose that this episode may provide a unique opportunity to elucidate a potential interaction between the solar dynamo and extreme solar flares.

1. Introduction

The Sun occasionally produces intense solar flares that sometimes accompany the ejection of energetic protons, described as solar proton events (SPEs). SPEs can potentially cause catastrophic damage to modern society by increasing the radiation levels around the Earth. For example, previous events have caused damage to spacecrafts (Shea et al., 1992) and increased the radiation exposure of airline crews and passengers (Fujita et al., 2021). Therefore, it is crucial to further understand how frequently and at which phases of solar activity large-scale SPEs may occur.

SPEs can be studied either by direct observation of cosmic-ray radiation or by

55   obtaining proxy-based data such as carbon-14 content in tree rings and/or

56   beryllium-10 stored in ice cores obtained from polar regions. Both carbon-14 and

57   beryllium-10 are radioactive isotopes produced by incident cosmic rays in the

58   atmosphere; thus, their content in tree rings or ice cores provides information on

59   past cosmic-ray events (Lal and Peters, 1967). While these isotopes are

60   constantly produced by galactic cosmic rays, whose flux is gradually changing

61   due to variations of the solar-wind magnetic field with timescales of decade or

62   longer, less energetic but massive radiations from SPE cause a rapid increase in

63   their production rate.

64   Based on carbon-14 records, Miyake et al. (2012; 2013) reported two extremely

65   large SPEs that occurred in 774–775 CE and 993–994 CE; the enhancement of

66   carbon-14 content was approximately 1%, and both were detected by the

67   ordinary precision of accelerator mass spectrometry (AMS) (0.2%–0.3%). Later,

68   the enhancement of carbon-14 on a similar scale was also reported for 660 BC

69   (O'Hare et al., 2019; Sakurai et al., 2020). For this event, detailed analyses have

70   suggested that this peak might have been produced by multiple, successive

71   SPEs occurring within a few years (Sakurai et al., 2020).

72   The frequency and the intensity of solar flares exhibit a power-law relationship

73 (e.g., Figure 4 of Maehara et al., 2015); thus, large-scale but comparably smaller

74 SPEs than 774–775 CE or 993–994 CE should have occurred more frequently in

75 the past. However, it is difficult to detect such smaller events with carbon-14 in

76 tree rings, as a transient enhancement in carbon-14 in the atmosphere is strongly

77 attenuated in the carbon cycle. A few possible candidates have been found but

78 are limited to those around 1052 CE and 1279 CE (Brehm et al., 2021), or around

79 5410 BC (Miyake et al., 2021).

80   Generally, SPEs occur when the Sun is active, as have been suggested for the

81 774–775 CE and 993–994 CE events; however, Brehm et al. (2021) have

82 suggested that SPEs could also occur during grand solar minima when solar

83 activity was extremely low for more than a few decades. During the grand minima,

84 the number of sunspots emerging on the solar surface becomes extremely small;

85 thus, there would be less chance for solar flares. However, it is known that

86 sunspots had caused solar flares even during the Maunder Minimum (1645–1715

87 CE), one of the periods of extremely low sunspot activity, and had brought some

88 aurorae events, although the event rate was extremely suppressed during that

89 time (Schlamminger, 1990).

90   However, it should be noted that galactic cosmic rays (GCRs) may also cause

91   an annual-scale rapid increase in carbon-14 around the grand minima

92   (Yamaguchi et al., 2010; Kataoka et al., 2012). Such an event may occur at the

93   minima of solar cycles during the grand solar minimum in the case where the

94   current sheet in the heliosphere, which plays an important role in the modulation

95   of cosmic rays, is extremely flattened. Such a condition may occur when the solar

96   surface is quiet—without any active region—and thus the tilt of the neutral line on

97   solar surface is reduced to ~0 degrees. Note that this effect is only prominent

98   when the polarity of the solar dipole magnetic field is negative, which is when

99   GCRs tend to come to the Earth along with the heliospheric current sheet by the

100   drift effect (Kota and Jokipii, 1983). Thus, such an event may occur only at every

101   other minima of solar cycles. The variation of beryllium-10 content obtained from

102   ice cores has suggested that the polarity reversal of the solar magnetic field had

103   been maintained even during the Maunder Minimum, with a slightly lengthened

104   cycle, and that the GCR flux had been increased by 30%–40% at every other

105   solar cycle minima (Yamaguchi et al., 2010; Kataoka et al., 2012).

106   Therefore, it is important to reconstruct the profile of solar cycles together with

107   the cosmic-ray events so that their origin can be identified. The reconstruction of

108   solar cycles also enables identifying the solar cycle dependence of large SPEs.

109   In order to determine the phases solar cycles at the times of cosmic-ray events,

110   it is helpful to obtain high-precision carbon-14 data—better than 0.1% (Miyahara

111   et al., 2021). Improving the measurement precision is also indispensable for

112   detecting relatively small SPEs, as well as precisely determining their intensity to

113   reveal their characteristics. In this paper, based on high-precision carbon-14

114   analyses, we report that multiple SPEs had occurred before the onset of the Wolf

115   grand minimum that occurred in the late 13th to the early 14th century (Figure 1a).

116   The solar cycle dependence of the events, as well as a possible relation to the

117   grand minimum, are presented.

118

119

120   **2. Materials and Methods**

121   **2.1. Measurement of carbon-14 content in annual tree rings**

122   In this study, we used tree-ring samples of asunaro (*Thujopsis dolabrata*)

123   excavated from the Shimokita Peninsula, Aomori Prefecture. Each of the annual

124   tree rings were cross-dated by dendrochronology (Hakozaki, 2012) and

125   absolutely dated by δ18O dendrochronology and carbon-14 spike-matching

126   (Hakozaki et al., 2016). The tree rings formed in 1250–1295 CE were then

127 separated and chemically treated to extract cellulose. We then produced graphite

128 as a target material and measured the carbon-14 content using the AMS at

129 Yamagata University in Japan (Tokanai et al., 2013; Moriya et al., 2019). In order

130 to achieve high-precision, we prepared four cathodes from each of the cellulose

131 samples, randomly loaded them onto the target wheel of the AMS, and repeated

132 measurements of 300 s for 14–24 cycles. We duplicated such measurements two

133 to three times to achieve a precision better than 0.08% in this study. We then

134 calculated the Δ14C values following the methodology described in a previous

135 study (Miyahara et al., 2021).

136

2.2. Estimation of carbon-14 production rate

138 For the determination of carbon-14 production rate, we used the 11-box carbon

139 cycle model introduced by Güttler et al. (2015). We first calculated the steady

140 state of the carbon cycle with the production rate of carbon-14 as 7.0 kg (total

141 amount for the stratosphere and the troposphere) for 200 kyrs, and then

142 continued the calculation for approximately 2000 years by adding a sinusoidal

143 curve with a period of 4400 years to reproduce the variation in carbon-14 content

144 (Reimer et al., 2020) caused by the long-term trend in geomagnetic field intensity.

145 The amplitude of the 4400-year cycle was adjusted so that the modeled Δ14C

146 value matched that of the measured value for the previous year of the cosmic-

147 ray candidate event. We then estimated the production rate of carbon-14 that can

148 reproduce the jump by injecting it into the model and by comparing the obtained

149 carbon-14 content in the troposphere with the high-precision data. Note that the

150 uncertainty of the carbon-14 data in the year before the event was propagated to

151 that of the event year to estimate the production anomaly within a range of 1 σ.

152 As any variations after the events may reflect decadal-scale solar activity

153 variations, they were not considered for the estimation of the intensities of the

154 events.

155

156 **2.3. Reconstruction of solar cycles**

157 In order to determine the profile of the solar cycles, we used a similar approach

158 as described in Miyahara et al. (2021). We constructed possible synthetic curves

159 of carbon-14 production rate caused by the decadal-scale variation of GCRs

160 associated with solar cycles, inputted them into the 11-box carbon cycle model,

161 and compared the modeled tropospheric carbon-14 content with the high-

162 precision carbon-14 data obtained in this study. For this calculation, we slightly

163 modified the initial setting mentioned in 2.2: the amplitude of 4400-year cycle was

164 adjusted so that the modeled $\Delta^{14}C$ matched the measured value in 1250 CE.

165 For the construction of the synthetic curves, we first synthesized possible

166 sunspot cycles and then obtained the corresponding cosmic-ray variations. For

167 synthesizing the sunspot curves, we assumed that the length of the ascending

168 phase did not exceed the length of the declining phase, following the

169 characteristics of sunspot cycles during the past 300 years. We set the resolution

170 of sunspot activity level as 20. For translating the sunspot cycles into cosmic-ray

171 cycles, we utilized a simple model estimated based on the relationship between

172 sunspot number and GCRs since 1953 CE as monitored by neutron monitors

173 (Supplementary Figure S1). We normalized and combined the Climax neutron

174 monitor data (http://cr0.izmir an.ru/clmx/main.htm) and the Oulu neutron monitor

175 data (http://cosmi crays.oulu.fi/) and compared them with sunspot numbers for

176 the two phases; the polarity of the solar dipole magnetic field was positive and

177 negative, respectively (Supplementary Figure S1c). We obtained approximate

178 equations and extrapolated the curves so that the calculation can be conducted

179 for a wide range of solar activity levels. Note that the Sun sometimes indicates

180 long-term variation in its magnetic activity not reflected in sunspot number, as

181 was the case for the deep activity minimum in 2008–2009. We therefore

182 extrapolated the curves down to a sunspot number of −150. As the decadal-scale

183 variation in carbon-14 content around 1265–1277 CE was significantly

184 suppressed compared to the previous/following cycle, we assumed that this cycle

185 corresponded to a period when the solar dipole magnetic field was positive.

186 Based on this assumption, we converted the sunspot curves into cosmic-ray

187 variations.

188 We input the synthetic curves into the carbon cycle model cycle by cycle. At

189 each cycle, $X^2 = \Sigma\ (\Delta^{14}C_{modeled} - \Delta^{14}C_{measured})^2/\sigma^2$ were calculated, and all the

190 synthetic curves that resulted in an X^2 below 1.69 (σ = 1.3) were adopted to

191 calculate the following cycle. As the obtained data do not fully cover the cycle

192 ending around 1259 CE, and the profile of the solar maximum in the

193 reconstruction may have a large ambiguity for this cycle, reconstructed curves

194 are shown only from around 1255 CE. Note that the reconstructed sunspot

195 activity level is dependent on the model of the GCR-sunspot relationship,

196 especially above 270 and below 0; therefore, the levels of sunspot maxima and

197 minima are reliable only in terms of relative magnitude.

198

11

199

3. Results and Discussion

Our newly obtained high-precision carbon-14 data, with a precision of 0.04%–

0.08%, substantially improved the understanding of solar activity around the

onset of the Wolf grand solar minimum in the 13th century. The data indicated that

there were three abrupt cosmic-ray events in a relatively short period of time just

before the onset of the Wolf minimum (Figure 1b). One of the events occurred in

1279–1280 CE, confirming one of the previously suggested SPE candidates by

Brehm et al. (2021) (Figure 2a), although the high-precision data revealed that

the increase in Δ14C was only approximately 0.3%, smaller than the 0.5%

increase suggested by Brehm et al. (2021). Another event was found to have

occurred in 1268–1269 CE (Figure 2b), 11 years before the above event. This

event was larger than the 1279–1280 CE event, and the offset of Δ14C was

approximately 0.45%. There was no increase from 1279 to 1280 CE in the

Brehm's record; instead, a jump of similar scale is seen—although statistically

insignificant—in the subsequent year. The discrepancy between the two records

may be explained either by (1) the relatively large uncertainty of the record by

Brehm et al. (2021) compared to the small signal or by (2) the tree species used

217   to obtain the data. The asunao tree used in this study is a conifer that is known

218   to start photosynthesis in early spring, and the majority of the produced

219   photosynthate is used for growth during the same year. On the contrary, the oak

220   used in the study of Brehms et al. (2021) is a deciduous tree that begins to sprout

221   in May and defoliate in late October, in which case the photosynthate of the

222   previous year is used for the growth of earlywood. It is therefore possible that the

223   carbon-14 signal is delayed by one year in the case of the deciduous tree. A

224   relatively small but possible SPE candidate was also found in the data in 1261–

225   1262 CE. An increase of 0.24% (~3 σ) was found in the carbon-14 content

226   together with a substantial decrease in 1263–1264 CE (Figure 2c), exceeding the

227   level that can be explained by solar cycles.

228   It is suggested by the carbon cycle modeling that the production rate of carbon-

229   14 caused by these three events was 5.6 ± 0.8 kg, 7.8 ± 1.2 kg, and 4.2 ± 1.4 kg,

230   respectively (see Supplementary Figure S2), corresponding to ~19%, ~27%, and

231   ~14% of the largest known SPE occurring in 774–775 CE (see Brehm et al., under

232   review, for the production rate of the 774–775 event). The event in 1268–1269

233   CE had been suggested to have caused a 9.2 ± 2.4 kg increase in carbon-14

234   production rate (Brehm et al., 2021), but the high-precision data allowed for

235 narrowing this uncertainty. The third event was the smallest extreme SPE

236 candidate detected by carbon-14 so far with sufficient statistical significance,

237 although further improvement in the measurement precision is desired for a better

238 estimation of the intensity.

239   Figure 3 shows the evolution of solar cycles around the events calculated using

240 the 11-box carbon cycle model (see 2.3), which suggests that the 1268–1269 CE

241 event and the 1279–1280 CE event had occurred at the declining phase of the

242 solar cycles, while the smallest event in 1261–1262 CE occurred at the maximum

243 of the solar cycle. The solar cycle dependence of the events suggests that they

244 were all caused by SPEs, rather than the galactic cosmic-ray enhancement

245 mentioned above. The 1279–1280 CE event had occurred at the early stage of

246 the declining phase, and the 1268–1269 CE event had occurred at the later stage

247 of the declining phase. It is noteworthy that the timings of ground level

248 enhancements (GLEs) captured by neutron monitors during the last 70 years

249 have shown a similar tendency. GLEs are abrupt increases in cosmic-ray intensity

250 associated with intense SPEs accompanying high-energy solar particles more

251 than a few hundred MeV. The solar cycle dependence of the timings of GLE

252 occurrence indicates that they increase as the number of sunspots increases, but

253 they are also frequent during the declining phase of solar cycles (see

254 Supplementary Figure S3). Note that GLE may also occur at the very end of the

255 solar cycle, associated with sunspot activities at low-latitude regions, as was the

256 case for the event of April 30, 1976 (Gopalswamy, 2012). A recent paper

257 suggested that active regions with a multipolar configuration—having a high

258 potential of triggering extreme solar flares—tended to occur at the solar activity

259 maximum and the declining phase of the solar cycle during the recent two cycles

260 (Solar Cycles 23 and 24) (Abramenko, 2021).

261 Interestingly, there has been a report of possible auroral activity on Feb 15th of

262 1269 CE in Korea (Abbott and Juhl, 2016). The record says that there was a white

263 cloud with a width of 3 degrees spread across the sky at night. Due to the gradual

264 change in the inclination angle of the geomagnetic field, it has been suggested

265 that the auroral zone had been closer to the East Asia around the 13th century

266 (Kataoka et al., 2021), and several aurorae were observed and recorded in Korea,

267 China, and Japan. Photosynthesis of the asunaro tree is active from April to

268 November and is most active around July to September (Hitsuma et al., 2012).

269 Given that the asunaro tree mainly uses the photosynthate from around April to

270 August for the growth of the correspondent year, a rapid jump from 1268 to 1269

271 CE does not contradict the time profile injection of protons in February of 1269 is

272 assumed. No auroral activity has been found around 1279–1280 CE and 1261–

273 1262 so far, except one suggested for Feb 9th of 1261 CE (Abbott and Juhl, 2016),

274 which is too early for the carbon-14 peak in 1262 CE; but the solar cycle

275 dependence of the events suggests that they were also caused by SPEs as

276 mentioned above.

277 The evolution of solar cycles deduced from the high-precision carbon-14

278 suggests that the peak around 1275 CE had been significantly suppressed

279 compared to the peak of the previous cycle. The end of the cycle then became

280 extremely weakened, beyond the sunspot minimum of the modern period. As

281 noted above, a sunspot level below zero implies a reduced solar activity more

282 than can be probed by the number of sunspots. A previous study suggested that

283 the Sun entered into the grand minimum state at around 1279 CE (Brehm et al.,

284 2021): detailed analyses of carbon-14 improve the estimation, suggesting that

285 the Wolf grand minimum had started around 1286 CE. It is noteworthy that the

286 total length of the two solar cycles was approximately 27 years, suggesting a

287 possibility that the length of the solar cycle had been longer than 11 years, as has

288 been suggested as the common characteristics before the onset of the grand

16

289 minimum (Miyahara et al., 2021), which is possibly associated with the reduction

290 in the speed of meridional circulation in the solar convection layer, although

291 further improvements to measurement precision are needed to precisely

292 determine the duration of each solar cycle.

293 The reconstructed solar cycles with a drastically decreasing activity trend

294 suggest that the SPEs found in this study had occurred during the transition time

295 of solar activity into the grand minimum state. From the viewpoint of solar dynamo

296 research, the Wolf minimum may provide a unique opportunity to discuss possible

297 interactions between the solar dynamo and extreme solar flares. Large flares tend

298 to occur at sunspots with complex topologies due to large available free energy

299 (e.g., Sammis et al., 2000). The fact that there were large flares during the drastic

300 transition phase of solar activity toward the Wolf minimum indirectly indicates that

301 the toroidal magnetic field in the solar interior had been passive to the turbulent

302 convection and was distorted significantly, leading to the generation of complex

303 sunspots and large SPEs (see also Abramenko, 2021). In this regard, our results

304 might constrain the status of the large-scale magnetic field and the convection in

305 the solar interior. Our results may also provide an implication of the evolution of

306 the Wolf minimum. Abramenko (2021) has shown that a large fraction of flaring

active regions in the late phase of the cycle violates the dynamo rules (e.g., Hale's law). Nagy et al. (2017) argue that a single "rogue" active region, i.e., an anti-Hale large sunspot pair, can significantly affect the construction of the polar magnetic field in the following minimum and the amplitude of the subsequent solar cycle. The sunspot pairs that caused the SPEs discussed in this study, especially those associated with the 1268–1269 CE and the 1279–1280 CE events, might therefore have contributed to the generation of the Wolf minimum. The excavation of sunspot descriptions in historical documents may give further insight in this regard.

4. Conclusions

We found three recurrent carbon-14 increases in the tree rings of 1262 CE, 1269 CE, and 1280 CE just before the onset of the Wolf grand solar minimum. Analyses of the production rate suggest that the intensities of these events were ~14%, ~27 %, and ~19% of that of the 774–775 CE event. The solar cycles reconstructed around the events suggest that they had occurred at the solar cycle maximum or at the declining phase of solar cycles, consistent with the

characterics of large-sized solar flares observed during the modern period. It

was suggested that they had occurred during a drastic transition time of solar

activity. Further exploration of large-scale SPEs and a detailed reconstruction of

solar cycles based on high-precision carbon-14 analyses may deepen our

understanding of the nature of large-scale solar flares and their possible relation

to the long-term variation of solar activity.

References

Shea, M. S., Smart, D. F., Allen, J. H., Wilkinson, D. C. (1992). Spacecraft

problems in association with episodes of intense solar activity and related

terrestrial phenomena during March 1991. IEEE Transactions on Nuclear

Science, 39(6), 1754–1760. https://doi.org/10.1109/23.211363

Fujita, M., Sato, T., Saito, S., Yamashiki, Y. (2021). Probabilistic risk assessment

of solar particle events considering the cost of countermeasures to reduce the

aviation radiation dose. Scientific Reports, 11, 17091.

https://doi.org/10.1038/s41598-021-95235-9

Lal, D., Peters, B. (1967). Cosmic ray produced activity on the earth. In: Sitte K. (ed.) Kosmische Strahlung II/cosmic rays II. Handbuch der Physik/Encyclopedia of Physics, vol 9/46/2. Springer, Berlin, Heidelberg. https://doi.org/10.1007/978-3-642-46079-17

Miyake, F., Nagaya, K., Masuda, K., Nakamura, T. (2012). A signature of cosmic-ray increase in AD 774-775 from tree rings in Japan. Nature, 486(7402), 240–242. https://doi.org/10.1038/nature11123

Miyake, F., Masuda, K., Nakamura, T. (2013). Another rapid event in the carbon-14 record of tree rings. Nature Communications, 4(1), 1748. https://doi.org/10.1038/ncomms287310.1038/ncomms2783

O'Hare, P., Mekhaldi, F., Adolphi, F., Raisbeck, G., Aldahan, A., Anderberg, E., et al. (2019). Multiradionuclide evidence for an extreme solar proton event around 2,610 BP (~660 BC). Proceedings of the National Academy of Sciences of the United States of America, 116(13), 5961–5966.

361 https://doi.org/10.1073/pnas.1815725116

362

363 Sakurai, H., Tokanai, F., Miyake, F., et al. (2020). Prolonged production of 14C

364 during the ~660 BCE solar proton event from Japanese tree rings. Scientific

365 Reports, 10, 660. https://doi.org/10.1038/s41598-019-57273-2

366

367 Maehara, H., Shibayama, T., Notsu, Y., Notsu, S., Honda, S., Nogami, D., et al.

368 (2015). Statistical properties of superflares on solar-type stars based on 1-min

369 cadence data. Earth, Planets and Space, 67, 59. https://doi.org/10.1186/s40623-

370 015-0217-z

371

372 Brehm, N., Bayliss, A., Christl, M., Synal, H. A., Adolphi, F., Beer, J., et al. (2021).

373 11-year solar cycles over the last millennium revealed by radiocarbon in tree rings.

374 Nature Geoscience, 14, 10–15. https://doi.org/10.1038/s41561-020-00674-0

375

376 Miyake, F., Panyushkina, I. P., Jull, A. J. T., Adolphi, F., Brehm, N., Helama, S., et

377 al. (2021). A single-year cosmic ray event at 5410 BCE registered in 14C of tree

378 rings. Geophysical Research Letters, 48, e2021GL093419.

379 https://doi.org/10.1029/2021GL093419

380

381 Schlamminger, L. (1990). Aurora borealis during the Maunder minimum. Monthly

382 Notices of the Royal Astronomical Society, 247, 67–69.

383

384 Yamaguchi, Y. T., Yokoyama, Y., Miyahara, H., Sho, K., Nakatsuka, T. (2010).

385 Synchronized northern hemisphere climate change and solar magnetic cycles

386 during the Maunder minimum. Proceedings of the National Academy of Sciences

387 of the United States of America, 107(48), 20697-20702.

388 https://doi.org/10.1073/pnas.1000113107

389

390 Kataoka, R., Miyahara, H., Steinhilber, F. (2012). Anomalous 10Be spikes during

391 the Maunder minimum: Possible evidence for extreme space weather in the

392 heliosphere.   Space   Weather,   10,   S11001,

393 https://doi.org/10.1029/2012SW000835.

394

395 Miyahara, H., et al. (2004). Cyclicity of solar activity during the Maunder minimum

396 deduced from radiocarbon content. Solar Physics, 224, 317–322

397

398 Kota, J., Jokipii, J. R., (1983). Effects of drift on the transport of cosmic rays. VI -

399 A three-dimensional model including diffusion. Astrophysical Journal, 265, 573–

400 581.

401

402 Miyahara, H., Tokanai, F., Moriya, T., Takeyama, M., Sakurai, H., Horiuchi, K.,

403 Hotta, H. (2021). Gradual onset of the Maunder Minimum revealed by high-

404 precision carbon-14 analyses. Scientific Reports, 11, 5482.

405 https://doi.org/10.1038/s41598-021-84830-5

406

407 Hakozaki, M. (2012). Dendrochronological study of coniferous buried forests in

408 the late Holocene. Ph.D. Dissertation. Tohoku University, Sendai, Miyagi,

409 Japan.(in Japanese)

410

411 Hakozaki, M., Nakamura, T., Ohyama, M., Kimura, J., Sano, M., Nakatsuka, T.

412 (2016). Verification for the chronological age of woody remains from the Nitta (1)

413 archaeological site in the Aomori city based on the AD774-775 14C-spike and

414 δ18O dendrochronology. Nagoya paper XXVII, 34–39.

415

Tokanai, F., Kato, K., Anshita, M., Sakurai, H., Izumi, A., Toyoguchi, T., et al.

(2013). Present status of YU-AMS system. Radiocarbon 55, 251–259.

Moriya, T., Takeyama, M., Sakurai, H., Umebayashi, T., Toyoguchi, T., Shiraishi,

T., et al. (2019). Status of the AMS system at Yamagata University. Nuclear

Instruments and Methods in Physics Research, B 439, 44–49.

Güttler, D., Adolphi, F., Beer, J., Bleicher, N., Boswijk, G., Christl, M., et al. (2015).

Rapid increase in cosmogenic 14C in AD 775 measured in New Zealand kauri

trees indicates short-lived increase in 14C production spanning both

hemispheres. Earth and Planetary Science Letters, 411, 290–297.

Reimer, P., Austin, W., Bard, E., Bayliss, A., Blackwell, P., Bronk Ramsey, C., et

al. (2020). The IntCal20 Northern Hemisphere Radiocarbon Age Calibration

Curve   (0–55   cal   kBP).   Radiocarbon,   62(4),   725–757.

https://doi.org/10.1017/RDC.2020.41

432

433 Brehm, N., Christl, M., Adolphi, F., Muscheler, R., Synal, H. A., Mekhaldi, F., et al.

434 Tree rings reveal two strong solar proton events in 7176 and 5259 BCE. Nature

435 Communications, under review.

436

437 Gopalswamy, N. (2012). Energetic particle and other space weather events of

438 solar cycle 24. In: Space weather: The space radiation environment: 11th

439 Annual International Astrophysics Conference, AIP Conference Proceedings

440 1500, 14–19.

441

442 Abramenko, V. I. (2021). Signature of the turbulent component of the solar

443 dynamo on active region scales and its association with flaring activity. Monthly

444 Notices of the Royal Astronomical Society, 507, 3698–3706.

445

446 Abbott, D. H., Juhl, R. (2016). New historical records and relationships among

447 14C production rates, abundance and color of low latitude auroras and sunspot

448 abundance. Advances in Space Research, 58, 2181–2246.

449

450 Kataoka, R., Nakano, S. (2021). Auroral zone over the last 3000 years. Journal

451   of   Space   Weather   and   Space   Climate,   11,   46.

452   https://doi.org/10.1051/swsc/2021030

453

454   Hitsuma, G., Han, Q., Chiba, Y. (2021). Photosynthesis and growth of Thujopsis

455   dolabrata var. hondai seedlings in the understory of trees with various

456   phenologies.   Journal   of   Service   Research,   17,   156–163.

457   http://doi.org/10.1007/s10310-011-0281-6

458

459   Sammis, I., Tang, F., Zirin, H. (2000). The dependence of large flare occurrence

460   on the magnetic structure of sunspots. The Astrophysical Journal, 540, 583–587.

461   https://doi.org/10.1086/309303

462

463   Nagy, M., Lemerle, A., Labonville, F., Petrovay, K., Charbonneau, P. (2017). The

464   effect of "rogue" active regions on the solar cycle. Solar Physics, 292, 167.

465   https://doi.org/10.1007/s11207-017-1194-0

466

467

472

473   **Data Availability Statement**

474   Datasets for this research are available at

475   https://doi.org/10.6084/m9.figshare.17096975.v1.

476

477   **Author Contributions**

478   H.M. designed the study. H.M., F.T., T.M., M.T., and K.H. conducted the 14C

479   measurements. M.O. performed the dating of tree-ring samples. H.M. and H.S.

480   performed data analyses and modeling. H.M., H.H., and H.S. wrote the

481   manuscript.

482

483   **Competing Interest**

484   The authors declare no competing interests.

485

486   **Supplementary Information**

487   Supplementary Information is available for this paper.

488
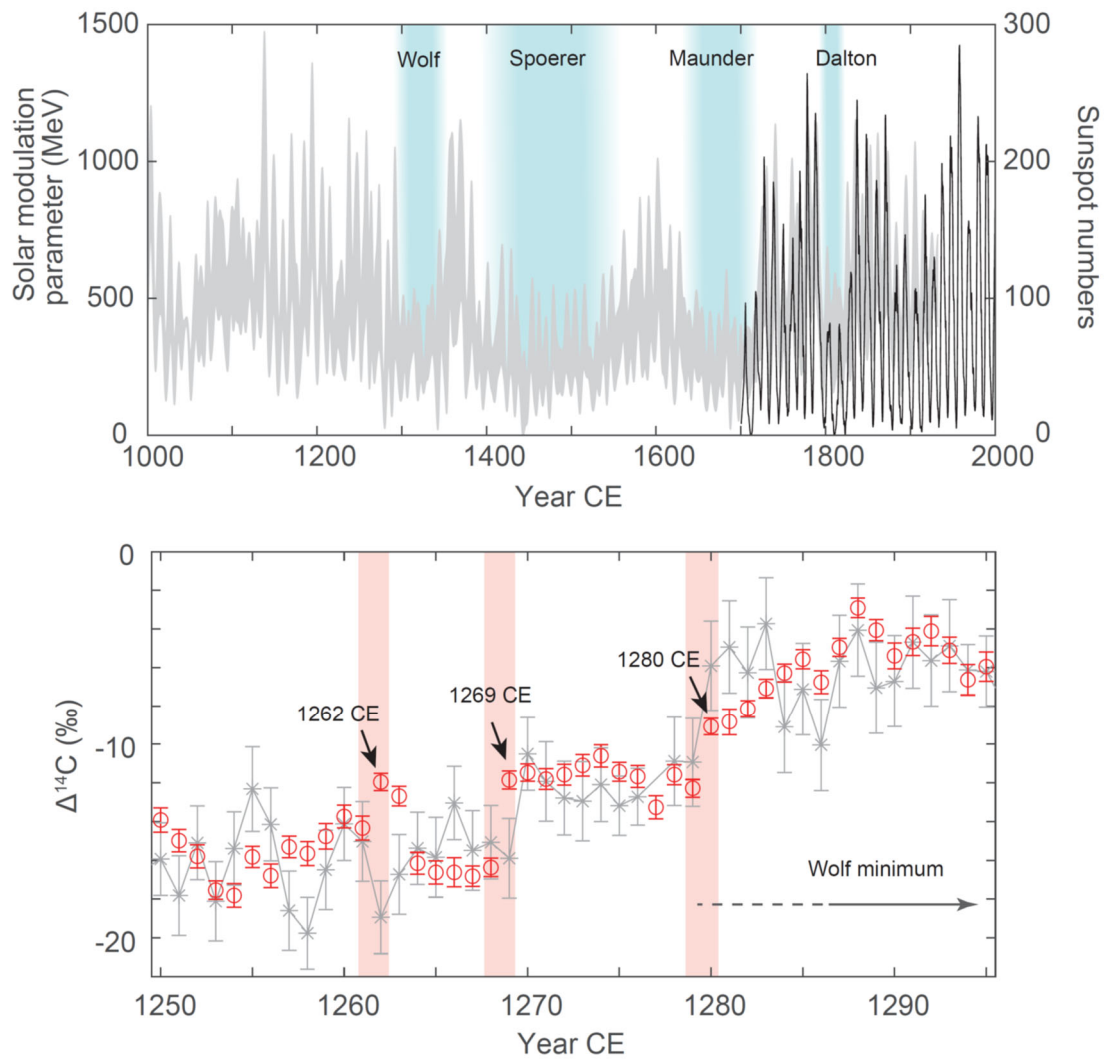
489

490   Figure 1. (a) Variation of solar modulation parameter for the past 1000 years

491   reconstructed by Brehm et al. (2021). Blue shaded areas indicate periods of

492   grand solar minima. (b) High-precision carbon-14 data for around the onset of the

493   Wolf Minimum. Red circles are the carbon-14 data obtained in this study. Gray

494   asterisks are the data by Brehm et al. (2021). Red shaded areas indicate the

495   periods when statistically significant jumps in carbon-14 content were recognized.
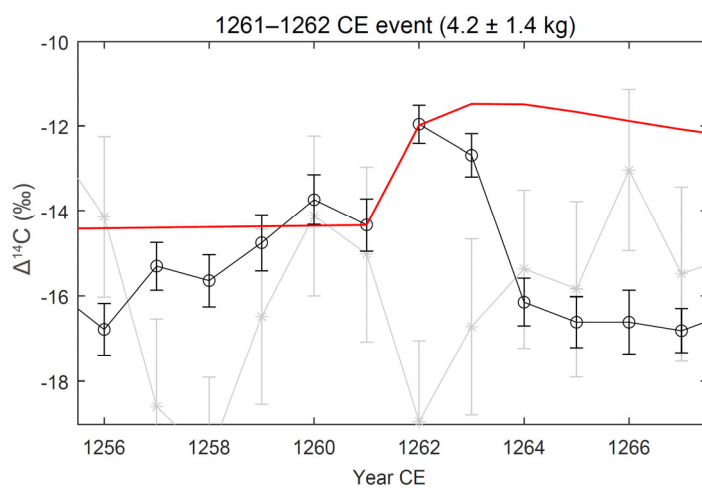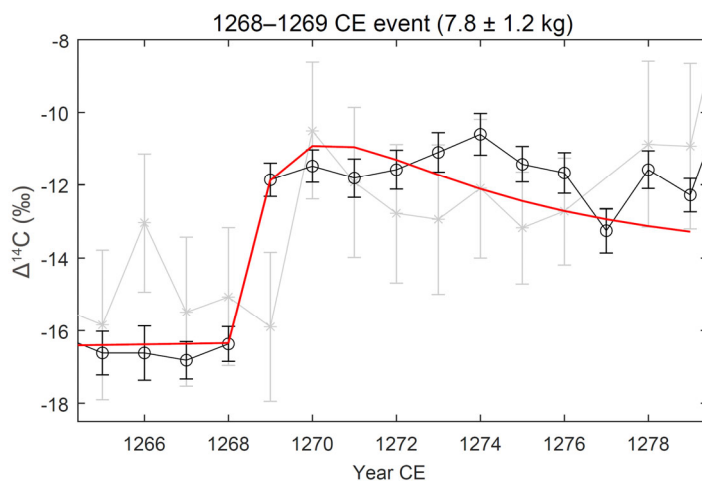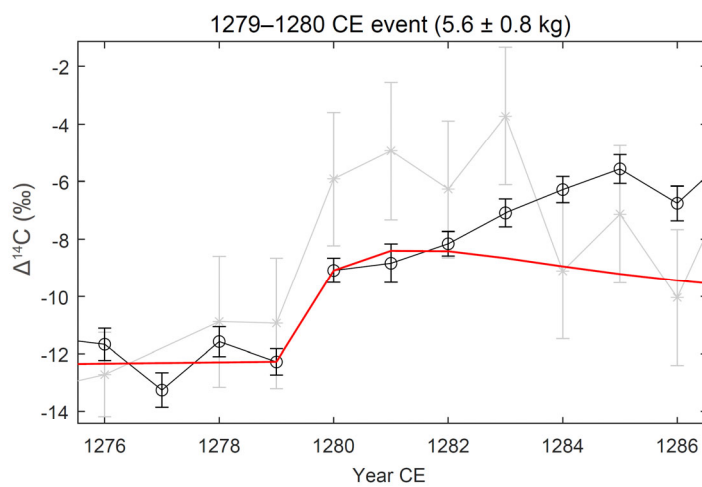
Figure 2. Time profile of carbon-14 content in tree rings around the SPE candidates: (a) 1279–1280 CE event, (b) 1268–1269 CE event, and (c) 1261–

499 1262 CE event. Black circles and gray asterisks are the carbon-14 data (same

500 as in Figure 1b). Red lines show the response of carbon-14 content to the carbon-

501 14 injections to the 11-box carbon cycle model. Note that solar cycle is not

502 considered in this calculation.

503
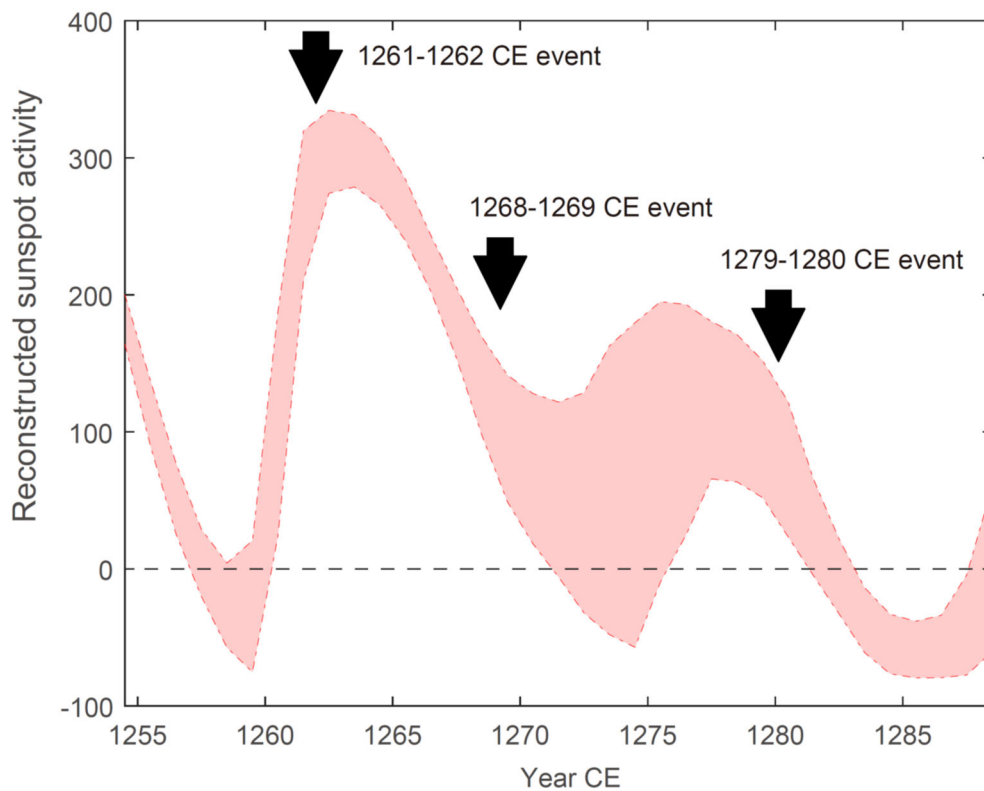
504

505 Figure 3. Reconstructed solar cycles around the carbon-14 enhancement events

506 with an uncertainty range of 1.3 σ. Arrows indicate the approximate timing of the

507 events found in this study.

508